ACS ORGANIC & INORGANIC Au
AN OPEN ACCESS JOURNAL OF THE AMERICAN CHEMICAL SOCIETY



pubs.acs.org/orginorgau
Article

# High-Throughput Determination of Stern–Volmer Quenching Constants for Common Photocatalysts and Quenchers

Rachel N. Motz, Alexandra C. Sun, Dan Lehnherr, and Serge Ruccolo*

Cite This: ACS Org. Inorg. Au 2023, 3, 266–273
Read Online

ACCESS | Metrics & More | Article Recommendations | Supporting Information

**ABSTRACT:** Mechanistic information on reactions proceeding via photoredox catalysis has enabled rational optimizations of existing reactions and revealed new synthetic pathways. One essential step in any photoredox reaction is catalyst quenching via photoinduced electron transfer or energy transfer with either a substrate, additive, or cocatalyst. Identification of the correct quencher using Stern–Volmer studies is a necessary step for mechanistic understanding; however, such studies are often cumbersome, low throughput and require specialized luminescence instruments. This report describes a high-throughput method to rapidly acquire a series of Stern–Volmer constants, employing readily available fluorescence plate readers and 96-well plates. By leveraging multichannel pipettors or liquid dispensing robots in combination with fast plate readers, the sampling frequency for quenching studies can be improved by several orders of magnitude. This new high-throughput method enabled the rapid collection of 220 quenching constants for a library of 20 common photocatalysts with 11 common quenchers. The extensive Stern–Volmer constant table generated greatly facilitates the systematic comparison between quenchers and can provide guidance to the synthetic community interested in designing and understanding catalytic photoredox reactions.

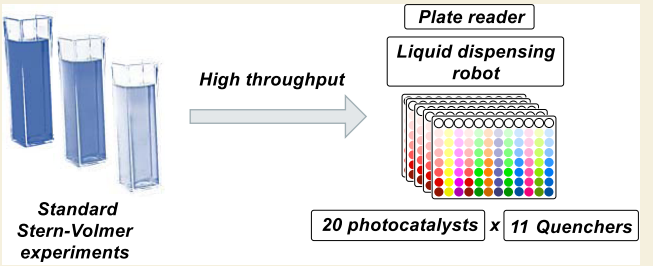


**KEYWORDS:** *photocatalysis, Stern–Volmer quenching, high-throughput experimentation, automation, quenching database*

## INTRODUCTION

Photocatalysis has emerged in the last decade as an important approach to perform new organic transformations.[1] These reactions include cyclizations, cross couplings, and amine and olefin functionalization and are routinely used in the synthesis of pharmacophores and drug-like molecules.[2−8] Typically, photocatalysis is driven by either energy transfer (EnT) or photoinduced electron transfer (PET) between the photocatalyst and a quencher, which forms a reactive radical or ionic species that initiates the desired reactivity.[9−11] The mechanism for PET occurs in one of two ways: (i) reductive quenching, whereby the photocatalyst is quenched through acceptance of an electron from a reductant or (ii) oxidative quenching, whereby the photocatalyst donates an electron to an oxidant (Figure 1A).[7] The quenching agent may be an integrated component of the transformation, such as one of the organic substrates or a cocatalyst or a sacrificial quencher that serves to convert the photocatalyst to a species that can oxidize or reduce the organic substrate, such as $O_2$ or alkyl amines.[11,12] Shedding light on quenching steps within a photoredox reaction is crucial to gain mechanistic insights;[13−17] this can include questions such as establishing which reaction component is acting as the main quencher and the magnitude of quenching that occurs under catalytically relevant conditions. In some cases, quenching studies have resulted in revisions of the originally proposed mechanisms,[18−21] while mechanistic understanding has led to designing improved photoefficiencies, faster reactions, and expanded scope.[22−24]

Emission quenching (also called Stern–Volmer) studies consist of measuring emission intensity fluctuations of the photocatalyst excited state in the presence of a quencher. In a typical Stern–Volmer study, a fluorometer is used to measure the emission intensity, and solutions of the photocatalyst with different concentrations of quenchers need to be prepared individually under a rigorously inert atmosphere to avoid the interference of oxygen quenching.[25] Such constraints have limited the prevalence of Stern–Volmer studies compared to the extensive body of work on photoredox catalysis. A fully automated continuous flow platform has been developed to facilitate data collection and reduce manual labor but remains low throughput and requires the construction of a homemade flow setup.[26] In parallel, several high-throughput technologies such as LED-illuminated 96-well plates as well as microfluidic and screening capabilities have been developed to allow for parallelized rapid discovery of new photoredox reactions.[27−29]

Received: May 17, 2023
Revised: June 13, 2023
Accepted: June 14, 2023
Published: June 29, 2023

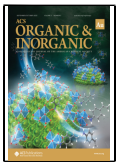





https://doi.org/10.1021/acsorginorgau.3c00019
ACS Org. Inorg. Au 2023, 3, 266–273

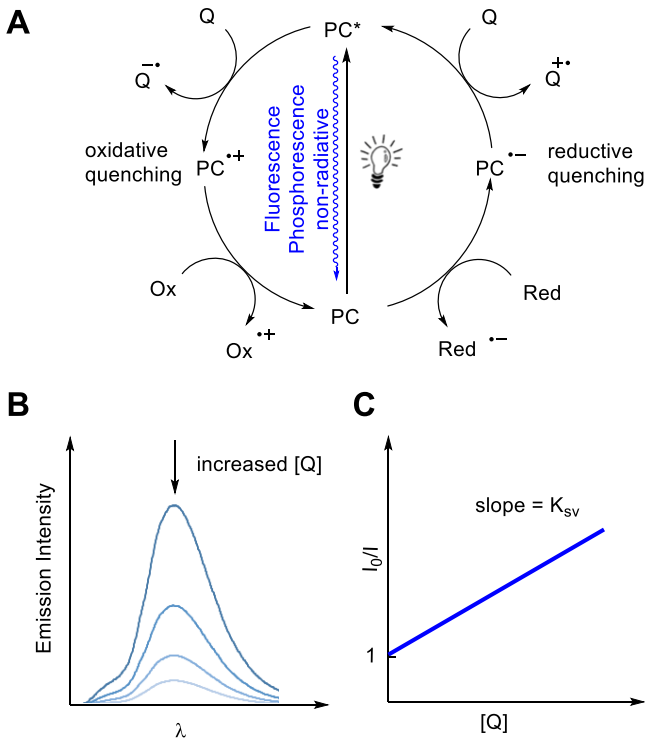


**Figure 1.** (A) General scheme for oxidative and reductive photocatalyst quenching. (B) Spectral changes from emission quenching. (C) Stern–Volmer analysis.

To keep up with the exponentially increasing chemical space for photocatalytic transformations, new workflows that enable Stern–Volmer data collection at a higher throughput need to be developed.

To that end, we have devised a protocol for the collection of Stern–Volmer quenching data using commercially available fluorescence plate readers and consumable 96-well plates. Plate readers are ubiquitous in biological studies and have been used in a variety of colorimetric and fluorometric assays,[30−32] as they allow for rapid (<1 min) reading of an entire 96-well plate. In our quenching studies, the use of well plates enables the collection of Stern–Volmer constants for one photocatalyst and up to 12 quenchers in less than a minute. We further expanded the throughput of this workflow by devising a protocol for a liquid handling robot to enable the automated dispensing of quenchers at increasing concentrations in a 96-well plate format. This allowed us to rapidly prepare multiple plates of 20 commonly used photocatalysts, and for each, measure the Stern–Volmer constants of 11 common quenchers.[2−9] The 220 quenching rate table generated opens the door for deeper data analysis of quenching trends and mechanisms, and we believe that it will be useful to the community interested in mechanistic understanding of photoredox catalysis.

## RESULTS AND DISCUSSION

In photoredox reactions, the first step in the photochemical cycle is excitation of the photocatalyst by a photon of the appropriate wavelength. Upon excitation, the photocatalyst can decay back to the ground state in a radiative (via photon emission, i.e., fluorescence or phosphorescence) or non-radiative way (heat) (Figure 1A).[33] In the presence of an increased concentration of a quencher, the photocatalyst excited state can also react via EnT or PET, which will compete with radiative decays and ultimately decrease photon emission (Figure 1B). The decrease in emission intensity is linked to the concentration of a quencher as described by the Stern–Volmer equation (eq 1)

$$\frac{I_0}{I} = 1 + k_q \tau_0 [Q] \tag{1}$$

where $I_0$ is the emission intensity in the absence of a quencher, $I$ is the intensity in the presence of a quencher, $k_q$ is the quenching constant, $\tau_0$ is the excited state lifetime, and $[Q]$ is the quencher concentration.[34] The product of $k_q$ and $\tau_0$ is often described as $K_{sv}$, the Stern–Volmer constant. $K_{sv}$ can be used to compare quenching rates between different quenchers (Figure 1C). The knowledge of $K_{sv}$ and $[Q]$ for all of the components of a reaction enables the ranking of quenching power and ultimate identification of the main quencher for the photocatalyst.

In a typical Stern–Volmer experiment, independent solutions of different concentrations of quenchers and a constant concentration of photocatalysts need to be prepared under a rigorously inert atmosphere, and the excitation intensity of each one must be measured separately to extract $I$ and build the Stern–Volmer plot. We decided to take advantage of the parallelization offered by 96-well plates to propose a Stern–Volmer plate design, which involves increasing the quencher concentration moving down a column, with a different quencher (or replicate) in each column (Figure 2). Multichannel pipettors enabled the rapid dispensing of each component across the entire plate. To maintain a strict inert atmosphere around the samples, the entire sample

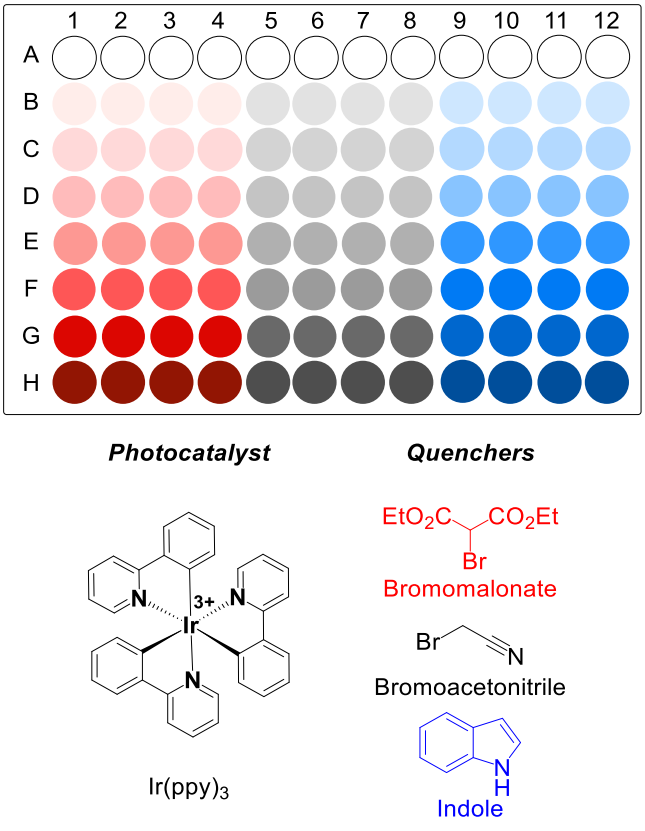


**Figure 2.** Plate design for workflow validation.



https://doi.org/10.1021/acsorginorgau.3c00019
ACS Org. Inorg. Au 2023, 3, 266−273

preparation and measurement were performed under an inert atmosphere inside a nitrogen-filled glovebox in constant purge mode. This was made possible by the small footprint of the fluorescence plate reader, which can easily be introduced into a glovebox. To validate this design, we sought to test our approach by comparing $K_{sv}$ values obtained with our workflow to values reported in the literature. We probed the quenching of (2,2′-bipyridine)bis[2-(pyridinyl-κN)phenyl-κC]iridium-(III) ($Ir(ppy)_3$) by diethylbromomalonate, bromoacetonitrile, and indole in dichloroethane (DCE) and observed similar trends in the quenching values, with diethylbromomalonate, exhibiting a higher $K_{sv}$ than bromoacetonitrile by a factor of 1.7 (in the original report, the factor is 2), and indole, showing virtually no quenching (Figure 3).[35]

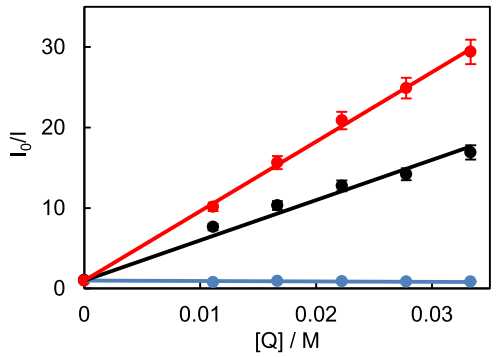


**Figure 3.** Stern–Volmer plot of $Ir(ppy)_3$ quenching by diethylbromomalonate (red circle solid), bromoacetonitrile (black circle solid), and indole (blue circle solid) at 375 nm with the linear fit (intercept set at 1).

However, we measured higher quenching constants overall by a factor of ∼2.[35] This difference is likely because of our ability to consistently maintain the sample in an inert atmosphere throughout the entire measurement using this workflow.

With this positive validation result in hand, we sought to showcase the magnitude of quenching data accessible through this high-throughput method. We decided to focus on generating Stern–Volmer constants for a library of commonly used photocatalysts and quenchers in a rapid fashion. We automated the plate preparation by writing a protocol to direct a liquid handling robot (Tecan Freedom EVO 100) to dispense the solutions of photocatalyst and quencher into 96-well plates. First, one photocatalyst was dispensed across the entire plate. We maintained the quencher concentration as the variable across rows and selected 12 widely used quenchers for the columns. With this design, one photocatalyst could be analyzed on a plate in less than one minute. The automated liquid dispensing allowed us to prepare plates for each of 20 common photocatalysts in <2 h entirely under an inert atmosphere (Figure 4) for a total of 1920 samples to generate 220 quenching constants.

The 12 quenchers were *N*,*N*-diisopropylethylamine, triethylamine, 4-methoxystyrene, Hantzsch ester, quinuclidine, bis(pinacolato)diboron, phenylacetic acid, tris(trimethylsylil)silanol, and potassium cyclohexyltrifluoroborate as reductive quenchers and di-*tert*-butyl peroxide and diethylbromomalonate as oxidative quenchers (sodium persulfate was included as well but exhibited low solubility in MeCN such that no quenching was measured and reported). These quenchers were

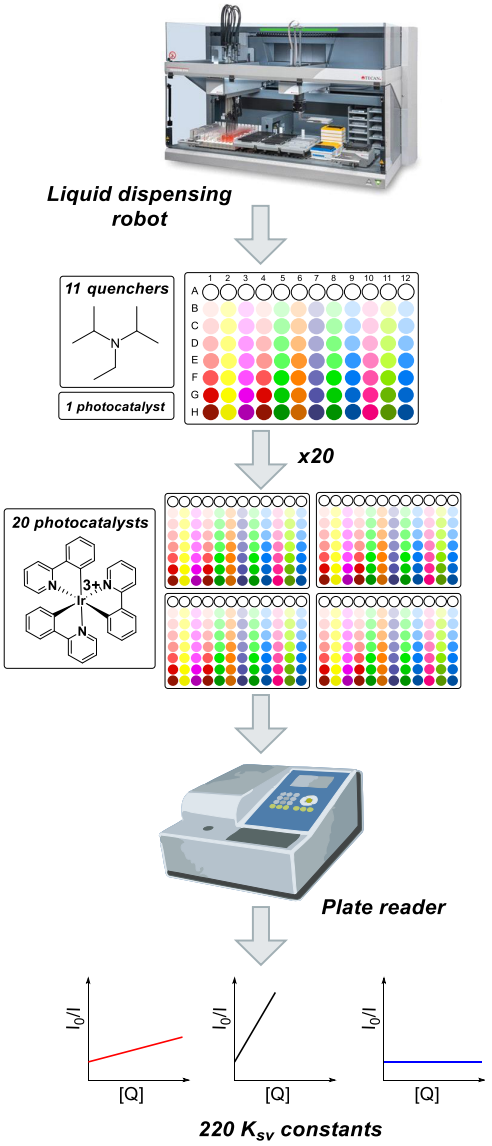


**Figure 4.** Semiautomated workflow for high-throughput Stern–Volmer studies.

selected for their wide use in many different photoredox reactions.[2,3,9,11] Trialkylamines are typically used as a sacrificial reductant to enable access to a highly reducing photocatalyst and, as such, are used in a wide range of reactions. The other reagents contain functional groups that will typically generate reactive radicals upon photocatalyst quenching and that will undergo the desired reactivity. The photocatalysts were selected to contain diverse chemical structures, such as cyanoarene-based photocatalysts, acridinium salts, ruthenium(II) complexes, iridium(III) complexes, and other miscellaneous organophotocatalysts. This selection varies not only in structures and photophysical properties but also in redox potentials while encompassing the most commonly used catalysts for photoredox reactions (Figure 5). The $K_{sv}$ values for different photocatalysts are reported in Table 1. For low $K_{sv}$ values, the entry is shown as <5. In such cases, higher concentrations of quenchers will be needed to determine $K_{sv}$.

Interestingly, we observed entries exhibiting negative deviations from linearity in their quenching profiles, mostly with Hantzsch ester (Figure 6) and diethylbromomalonate.


https://doi.org/10.1021/acsorginorgau.3c00019
ACS Org. Inorg. Au 2023, 3, 266–273

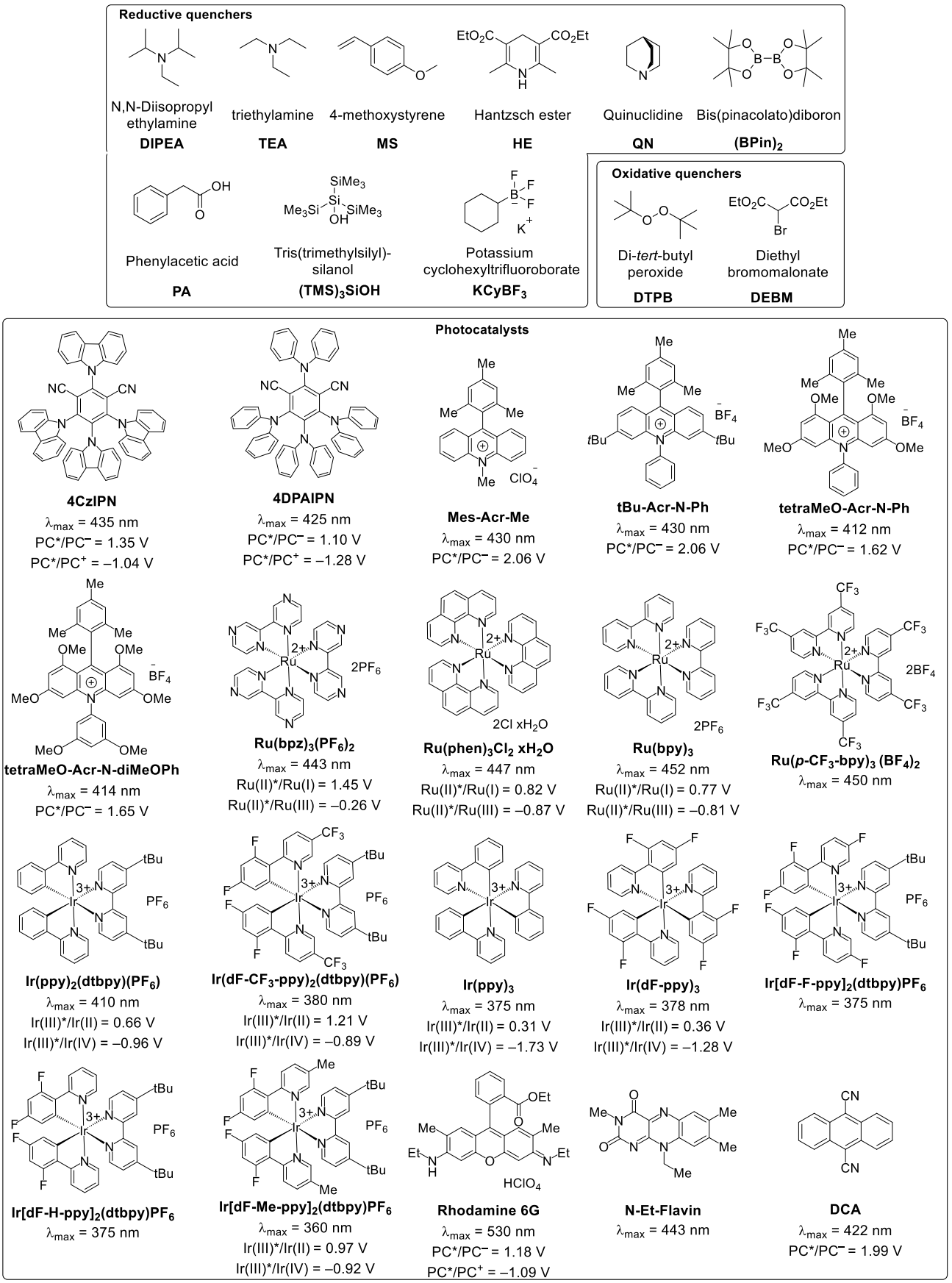


**Figure 5.** Quenchers and photocatalysts for the quenching studies. $\lambda_{max}$ is the absorption maximum for the photocatalyst and below are reported the potential for the redox couples of the excited photocatalyst.



https://doi.org/10.1021/acsorginorgau.3c00019
ACS Org. Inorg. Au 2023, 3, 266–273

**Table 1. $K_{sv}$ between Catalyst and Quencher Collection Reported in $M^{-1}$[a]**

| | | quenchers | | | | | | | | | | |
|---|---|---|---|---|---|---|---|---|---|---|---|---|
| | | DIPEA | TEA | MS | HE | QN | (Bpin)2 | PA | $(TMS)_3SiOH$ | $KCyBF_3$ | DTBP | DEBM |
| photocatalysts | 4CzIPN | 254 | 89 | 21 | 201 | 219 | 13 | <5 | 26 | <5 | <5 | <5 |
| | 4DPAIPN | 11 | <5 | <5 | <5 | <5 | <5 | 8 | <5 | <5 | <5 | 63 |
| | Mes-Acr-Me | 73 | 54 | 97 | <5 (b) | 104 | <5 | <5 | 169 | 77 | <5 | <5 |
| | $^t$Bu-Acr-N-Ph | 196 | 111 | 229 | 315 (b,c) | 205 | <5 | <5 | 191 | 126 | <5 | <5 |
| | tetraMeO-Acr-N-Ph | 58 | 55 | 46 | 717 (b,c) | 63 | 40 | 14 | 44 | 27 | 11 | (a) |
| | tetraMeO-Acr-N-diMeOPh | 64 | 52 | 51 | 1047 (b,c) | 77 | 48 | 30 | 38 | 26 | <5 | (a) |
| | $Ru(bpz)_3(PF_6)_2$ | 2379 | 357 | 59 | 1640 | 1742 | 9 | <5 | 83 | <5 | <5 | <5 |
| | $Ru(phen)_3Cl_2xH_2O$ | 13 | <5 | <5 | <5 | <5 | <5 | <5 | <5 | <5 | (a) | (a) |
| | $Ru(bpy)_3(PF_6)_2$ | 30 | <5 | 21 | 25 | 20 | 25 | <5 | 25 | <5 | <5 | <5 |
| | $Ru(p\text{-}CF_3\text{-}bpy)_3(BF_4)_2$ | 1164 | 77 | <5 | 982 | 294 | <5 | <5 | 24 | 17 | <5 | <5 |
| | $Ir(ppy)_2(dtbpy)(PF_6)$ | 501 | 50 | 17 | 318 | 28 | <5 | <5 | <5 | <5 | <5 | <5 |
| | $Ir(dF\text{-}CF_3\text{-}ppy)2(dtbpy)(PF_6)$ | 6085 | 1642 | 4941 | (a,b) | 3508 | <5 | <5 | 10 | <5 | <5 | <5 |
| | $Ir(ppy)_3$ | <5 | <5 | <5 | 5939 (b,c) | <5 | <5 | <5 | <5 | <5 | <5 | 1495 |
| | $Ir(dF\text{-}ppy)_3$ | <5 | <5 | 689 | <5 (b) | <5 | <5 | <5 | <5 | <5 | <5 | 291 |
| | $Ir(dF\text{-}F\text{-}ppy)_2(dtbpy)PF_6$ | 4286 | 1377 | 3660 | (a,b) | 2957 | <5 | <5 | 23 | <5 | <5 | <5 |
| | $Ir(dF\text{-}H\text{-}ppy)_2(dtbpy)PF_6$ | 54 | 53 | 64 | <5 (b) | <5 | <5 | <5 | <5 | <5 | <5 | <5 |
| | $Ir(dF\text{-}Me\text{-}ppy)_2(dtbpy)PF_6$ | 6212 | 677 | 619 | <5 (b) | 928 | <5 | <5 | <5 | <5 | <5 | <5 |
| | Rhodamine 6G | 43 | <5 | <5 | <5 | <5 | <5 | <5 | 10 | 8 | <5 | <5 |
| | N-Et-Flavinium | 87 | 34 | 93 | 88 | 121 | <5 | <5 | 548 | <5 | <5 | 17 |
| | DCA | 259 | 179 | 278 | 104 (b) | 219 | <5 | 15 | 344 | <5 | <5 | <5 |

[a](a) Nonlinear quenching, (b) absorbance overlap between the quencher and photocatalyst, and (c) fit with the Lehrer equation.

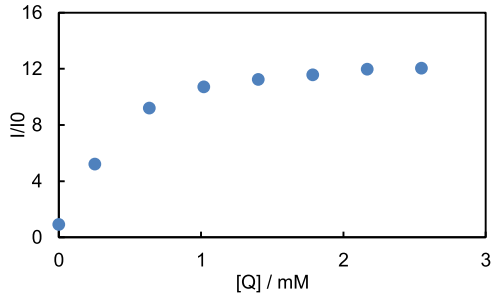


**Figure 6.** Nonlinear quenching of $Ir(ppy)_3$ by HE.

This type of behavior has been attributed to the presence of different conformers for the photocatalyst, which gives rise to fractional accessibility of the fluorophore.[36] Some cases can be treated using a modified Stern−Volmer equation, namely, the Lehrer equation.[37] It should be noted that the Hantzsch ester, unlike the other quenchers, also has a non-negligeable absorbance up to 400 nm and emits at 450 nm,[38] which overlaps with the absorbance and emission of a few of the selected photocatalysts, thereby creating an inner filter effect, which interferes with the Stern−Volmer measurement. Therefore, data for this particular quencher might not reflect the true photocatalyst quenching rate.

Overall, we observed strong quenching from trialkylamines with typically oxidative excited photocatalysts (Figure 7A), which is unsurprising considering their wide use as quenchers in many photoredox reactions. DIPEA is the substrate that exhibits quenching with most photocatalysts in the collection. Conversely, oxidative quenchers like diethylbromomalonate tend to only react with strongly reducing photocatalysts such as $Ir(ppy)_3$. However, further data analysis of $K_{sv}$ values of the quenchers in relation to the oxidation potential of the photocatalyst excited state shows that, interestingly, these two entities are not necessarily related. For example, quenching values for triethylamine show no clear correlation between $K_{sv}$ and excited state oxidation potential (Figure 7B). Other phenomena such as pH, binding events, exciplex formation, or hydrogen bonding have been shown to influence quenching.[17,23] Solvent effects also have a role, as illustrated by the 1.7-fold higher $K_{sv}$ between

$Ir(ppy)_3$ and diethylbromomalonitrile in acetonitrile compared to that in DCE. Additionally, phenylacetic acid showed very little quenching with all photocatalysts, but the quenching rate for this specific quencher is likely dependent on pH with the deprotonated carboxylate being more susceptible to oxidation.[4,39] An interesting quencher is $(TMS)_3SiOH$, which has been used recently in several metallophotoredox reactions[1,40] and which shows noticeable quenching patterns. Indeed, while most reported systems including $(TMS)_3SiOH$ involve Ir photocatalysts, we can observe much higher quenching with acridiniums and organocatalysts, such as N-Et-Flavin and DCA. These photocatalysts could therefore outperform Ir in systems relying on this quencher. Interestingly, two photocatalysts, namely, tetraMeO-Acr-N-Ph and tetraMeO-Acr-N-diMeOPh, show some degree of quenching with all of the quenchers tested (Figure 7C), which might explain their increased use as versatile photocatalysts.[9] On the contrary, photocatalysts, such as $Ru(phen)_3Cl_2$ and $Ru(bpy)_3(PF6)_2$, one of the most important photocatalysts that launched the entire field of photoredox catalysis,[11] exhibit fairly poor quenching with most substrates. This observation could partially explain its decline in usage against more reactive Ir photocatalysts, although it should be noted that many other factors beyond photocatalyst quenching impact photocatalytic processes and can determine the failure or success of a photocatalyst.

In conclusion, we demonstrated the use of a high-throughput workflow for the measurements of Stern−Volmer quenching constants using commercially available fluorescence plate readers and 96-well plates. We validated the method by comparing the results to reported quenching values. Automatization of the liquid dispensing step allowed for the rapid preparation and analysis of the Stern−Volmer quenching for a


https://doi.org/10.1021/acsorginorgau.3c00019
ACS Org. Inorg. Au 2023, 3, 266−273

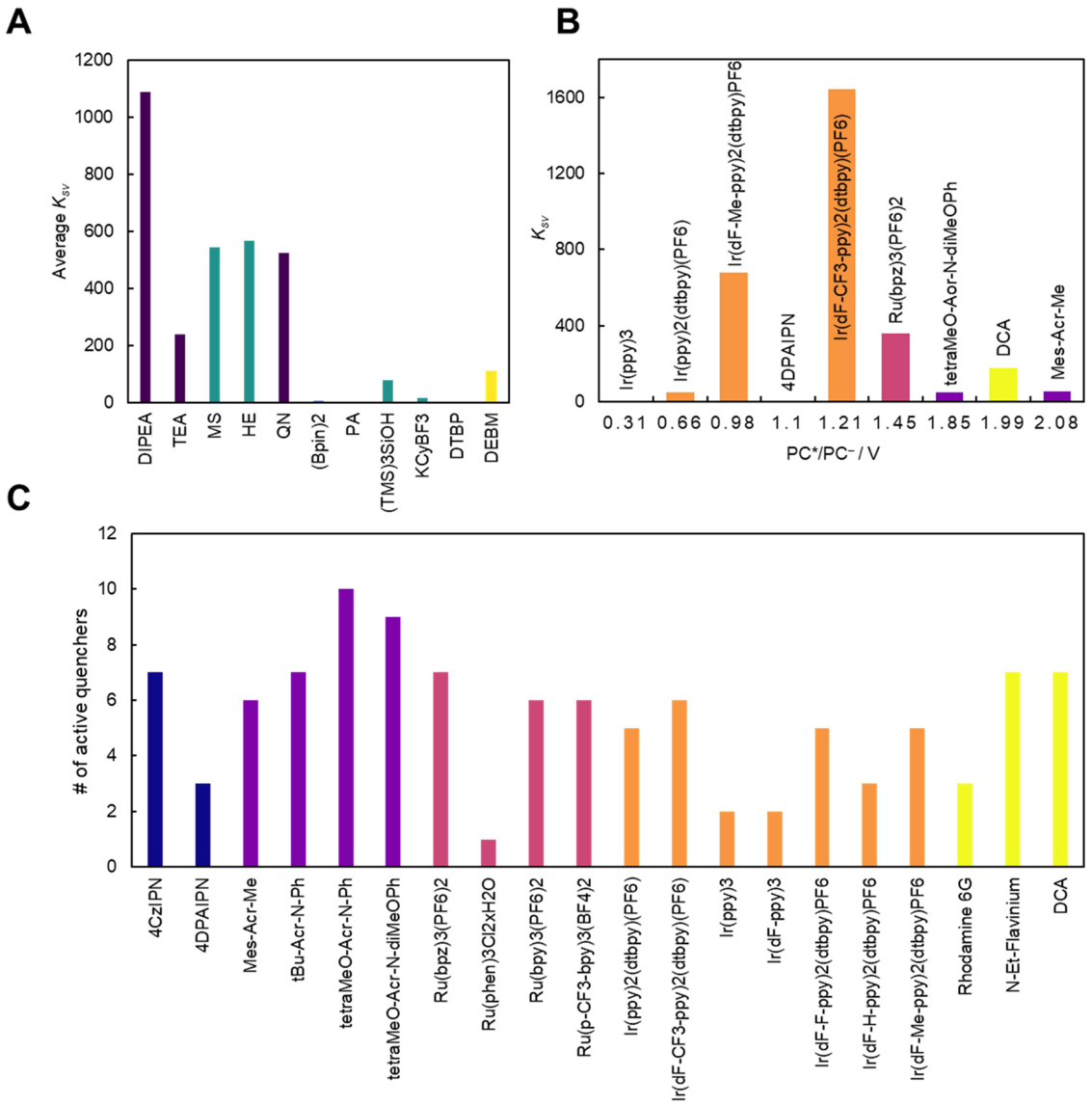


**Figure 7.** (A) Comparison of the average $K_{sv}$ over all of the photocatalysts for each quencher. (B) Plot of $K_{sv}$ against the photocatalyst excited state potential for triethylamine. (C) Number of quenchers with >5 $K_{sv}$ for each photocatalyst. Color coding: trialkylamines (purple circle solid), other reductive quenchers (teal circle solid), oxidative quenchers (yellow circle solid), cyanoarenes (blue circle solid), acridiniums (purple circle solid), Ru(II) complexes (maroon circle solid), Ir(III) complexes (orange circle solid), and miscellaneous organic photocatalysts (light yellow circle solid).

collection of common photocatalysts and quenchers. We believe that this workflow enables a consistent and rapid collection of quenching constants with readily available instrumentation, thereby finally bringing Stern−Volmer studies to the same level of high-throughput capabilities as those for reaction discovery for photoredox catalysis. We believe that this method as well as the data generated is truly enabling for the community interested in mechanistic understanding of photoredox reactions.

## EXPERIMENTAL SECTION

### Chemicals and Materials

Unless stated otherwise, all of the reagents and solvents were purchased from commercial suppliers (Acros, Merck Millipore Sigma, TCI America, Fisher Scientific, etc.) and were of the highest analytical purity. UPLC grade solvents were used for all experiments. All operations were performed inside a $N_2$-filled glovebox. For the high-throughput experiments, 96-well UV-star microplates (part number 655809) were used. For the validation experiments, the microplate used was a 96-well quartz microplate (part number 730−009−44) due to solvent incompatibility. Emission measurements were performed with a Molecular Devices Spectramax M5, and the data was compiled on SoftMax Pro 6.5.1. Liquid handling was performed on a Tecan Freedom EVO 100 outfitted with an eight-channel liquid handler (LiHa) with Teflon-coated fixed tips.

### Microplate Preparation

20 mM stock solutions of individual quenchers and 10 $\mu$M stock solution of photocatalyst were prepared. The plate was designed such that one photocatalyst was dispensed across an entire plate and each column contained a different quencher. For example, 100 $\mu$L of photocatalyst solution was dispensed in all 96 wells. Then, in each row, going from rows A to H, 0, 10, 25, 40, 55, 70, 85, and 100 $\mu$L of quencher solution was added, respectively, with a different quencher in each column. Then, going from rows A to H, 100, 90, 75, 60, 45, 30, 15, and 0 $\mu$L of acetonitrile was added, respectively, to make a total of 200 $\mu$L in each well. The microplate was sealed with a clear silicon mat and was placed in the microplate reader. The excitation wavelength was either taken from the literature value for each photocatalyst or was determined experimentally from an absorption


https://doi.org/10.1021/acsorginorgau.3c00019
ACS Org. Inorg. Au 2023, 3, 266−273

and fluorescence spectrum measured with the plate reader. The emission data was then exported to Excel and fit to the Stern−Volmer equation using least squares regression with $y$-intercept set to 1. The slope values (i.e., quenching constants) were filtered by magnitude and by $R^2$ value to constrain the data to the observation of significant linear quenching. Plots with noticeable but nonlinear quenching were tested for outliers (two standard deviations away from the line of the best fit) and/or improved fit with the Lehrer equation.

## ■ ASSOCIATED CONTENT

### Data Availability Statement

The data underlying this study are available in the published article and its Supporting Information.

### Supporting Information

The Supporting Information is available free of charge at https://pubs.acs.org/doi/10.1021/acsorginorgau.3c00019.

The supporting information contains the Tecan script for the automated dispensing and the raw emission data (PDF)

## ■ AUTHOR INFORMATION


### Corresponding Author

**Serge Ruccolo** − *Process Research and Development, Merck & Co., Inc., Rahway, New Jersey 07065, United States;* orcid.org/0000-0002-4297-2751; Email: serge.ruccolo@merck.com

### Authors

**Rachel N. Motz** − *Process Research and Development, Merck & Co., Inc., Rahway, New Jersey 07065, United States*

**Alexandra C. Sun** − *Process Research and Development, Merck & Co., Inc., Rahway, New Jersey 07065, United States;* orcid.org/0000-0002-5583-8068

**Dan Lehnherr** − *Process Research and Development, Merck & Co., Inc., Rahway, New Jersey 07065, United States;* orcid.org/0000-0001-8392-1208

Complete contact information is available at: https://pubs.acs.org/10.1021/acsorginorgau.3c00019


### Author Contributions

This manuscript was written through contributions of all authors. All authors have given approval to the final version of the manuscript.

### Notes

The authors declare no competing financial interest.

## ■ ACKNOWLEDGMENTS

Michael Shevlin, Aaron Whittaker, Heather Wang, Erik Regalado, Shasha Li, and Imad Haidar Ahmad are thanked for their contribution. The MFT Chemistry Recruiting Team, Shanley Lenart, and the NGN Intern Mentoring Program are thanked for their support. Prof. Robert Knowles is thanked for helpful advice and discussion. Kate Maldjian is thanked for help with graphics.

## ■ REFERENCES


(1) Bell, J. D.; Murphy, J. A. Recent Advances in Visible Light-Activated Radical Coupling Reactions Triggered by (i) Ruthenium, (Ii) Iridium and (Iii) Organic Photoredox Agents. *Chem. Soc. Rev.* **2021**, *50*, 9540−9685.

(2) Shaw, M. H.; Twilton, J.; MacMillan, D. W. C. Photoredox Catalysis in Organic Chemistry. *J. Org. Chem.* **2016**, *81*, 6898−6926.

(3) Chan, A. Y.; Perry, I. B.; Bissonnette, N. B.; Buksh, B. F.; Edwards, G. A.; Frye, L. I.; Garry, O. L.; Lavagnino, M. N.; Li, B. X.; Liang, Y.; Mao, E.; Millet, A.; Oakley, J. V.; Reed, N. L.; Sakai, H. A.; Seath, C. P.; MacMillan, D. W. C. Metallaphotoredox: The Merger of Photoredox and Transition Metal Catalysis. *Chem. Rev.* **2022**, *122*, 1485−1542.

(4) Murray, P. R. D.; Cox, J. H.; Chiappini, N. D.; Roos, C. B.; McLoughlin, E. A.; Hejna, B. G.; Nguyen, S. T.; Ripberger, H. H.; Ganley, J. M.; Tsui, E.; Shin, N. Y.; Koronkiewicz, B.; Qiu, G.; Knowles, R. R. Photochemical and Electrochemical Applications of Proton-Coupled Electron Transfer in Organic Synthesis. *Chem. Rev.* **2022**, *122*, 2017−2291.

(5) Bonfield, H. E.; Knauber, T.; Lévesque, F.; Moschetta, E. G.; Susanne, F.; Edwards, L. J. Photons as a 21st Century Reagent. *Nat. Commun.* **2020**, *11*, No. 804.

(6) Kwon, K.; Simons, R. T.; Nandakumar, M.; Roizen, J. L. Strategies to Generate Nitrogen-Centered Radicals That May Rely on Photoredox Catalysis: Development in Reaction Methodology and Applications in Organic Synthesis. *Chem. Rev.* **2022**, *122*, 2353−2428.

(7) Skubi, K. L.; Blum, T. R.; Yoon, T. P. Dual Catalysis Strategies in Photochemical Synthesis. *Chem. Rev.* **2016**, *116*, 10035−10074.

(8) Candish, L.; Collins, K. D.; Cook, G. C.; Douglas, J. J.; Gómez-Suárez, A.; Jolit, A.; Keess, S. Photocatalysis in the Life Science Industry. *Chem. Rev.* **2022**, *122*, 2907−2980.

(9) Romero, N. A.; Nicewicz, D. A. Organic Photoredox Catalysis. *Chem. Rev.* **2016**, *116*, 10075−10166.

(10) Arias-Rotondo, D. M.; McCusker, J. K. The Photophysics of Photoredox Catalysis: A Roadmap for Catalyst Design. *Chem. Soc. Rev.* **2016**, *45*, 5803−5820.

(11) Prier, C. K.; Rankic, D. A.; MacMillan, D. W. C. Visible Light Photoredox Catalysis with Transition Metal Complexes: Applications in Organic Synthesis. *Chem. Rev.* **2013**, *113*, 5322−5363.

(12) Wu, C.; Jung, K.; Ma, Y.; Liu, W.; Boyer, C. Unravelling an Oxygen-Mediated Reductive Quenching Pathway for Photopolymerisation under Long Wavelengths. *Nat. Commun.* **2021**, *12*, No. 478.

(13) Stanek, F.; Pawlowski, R.; Morawska, P.; Bujok, R.; Stodulski, M. Dehydrogenation and $\alpha$-Functionalization of Secondary Amines by Visible-Light-Mediated Catalysis. *Org. Biomol. Chem.* **2020**, *18*, 2103−2112.

(14) Jin, J.; MacMillan, D. W. C. Alcohols as Alkylating Agents in Heteroarene C−H Functionalization. *Nature* **2015**, *525*, 87−90.

(15) Yue, H.; Zhu, C.; Kancherla, R.; Liu, F.; Rueping, M. Regioselective Hydroalkylation and Arylalkylation of Alkynes by Photoredox/Nickel Dual Catalysis: Application and Mechanism. *Angew. Chem., Int. Ed.* **2020**, *59*, 5738−5746.

(16) Tlahuext-Aca, A.; Garza-Sanchez, R. A.; Glorius, F. Multicomponent Oxyalkylation of Styrenes Enabled by Hydrogen-Bond-Assisted Photoinduced Electron Transfer. *Angew. Chem., Int. Ed.* **2017**, *56*, 3708−3711.

(17) Buzzetti, L.; Crisenza, G. E. M.; Melchiorre, P. Mechanistic Studies in Photocatalysis. *Angew. Chemie - Int. Ed.* **2019**, *58*, 3730−3747.

(18) Sun, R.; Qin, Y.; Nocera, D. G. General Paradigm in Photoredox Nickel-Catalyzed Cross-Coupling Allows for Light-Free Access to Reactivity. *Angew. Chem., Int. Ed.* **2020**, *59*, 9527−9533.

(19) Qin, Y.; Sun, R.; Gianoulis, N. P.; Nocera, D. G. Photoredox Nickel-Catalyzed C-S Cross-Coupling: Mechanism, Kinetics, and Generalization. *J. Am. Chem. Soc.* **2021**, *143*, 2005−2015.

(20) Spielvogel, E. H.; Stevenson, B. G.; Stringer, M. J.; Hu, Y.; Fredin, L. A.; Swierk, J. R. Insights into the Mechanism of an Allylic Arylation Reaction via Photoredox-Coupled Hydrogen Atom Transfer. *J. Org. Chem.* **2022**, *87*, 223−230.

(21) Till, N. A.; Tian, L.; Dong, Z.; Scholes, G. D.; MacMillan, D. W. C. Mechanistic Analysis of Metallaphotoredox C-N Coupling: Photocatalysis Initiates and Perpetuates Ni(I)/Ni(III) Coupling Activity. *J. Am. Chem. Soc.* **2020**, *142*, 15830−15841.

(22) Qin, Y.; Zhu, Q.; Sun, R.; Ganley, J. M.; Knowles, R. R.; Nocera, D. G. Mechanistic Investigation and Optimization of Photoredox Anti-Markovnikov Hydroamination. *J. Am. Chem. Soc.* **2021**, *143*, 10232−10242.
(23) Ruccolo, S.; Qin, Y.; Schnedermann, C.; Nocera, D. G. General Strategy for Improving the Quantum Efficiency of Photoredox Hydroamidation Catalysis. *J. Am. Chem. Soc.* **2018**, *140*, 14926−14937.
(24) Cismesia, M. A.; Yoon, T. P. Characterizing Chain Processes in Visible Light Photoredox Catalysis. *Chem. Sci.* **2015**, *6*, 5426−5434.
(25) Kautsky, H. Quenching of Luminescence by Oxygen. *Trans. Faraday Soc.* **1939**, *35*, 216−219.
(26) Kuijpers, K. P. L.; Bottecchia, C.; Cambié, D.; Drummen, K.; König, N. J.; Noël, T. A Fully Automated Continuous-Flow Platform for Fluorescence Quenching Studies and Stern−Volmer Analysis. *Angew. Chem., Int. Ed.* **2018**, *57*, 11278−11282.
(27) Tay, N. E. S.; Lehnherr, D.; Rovis, T. Photons or Electrons? A Critical Comparison of Electrochemistry and Photoredox Catalysis for Organic Synthesis. *Chem. Rev.* **2022**, *122*, 2487−2649.
(28) Hopkinson, M. N.; Gómez-Suárez, A.; Teders, M.; Sahoo, B.; Glorius, F. Accelerated Discovery in Photocatalysis Using a Mechanism-Based Screening Method. *Angew. Chem., Int. Ed.* **2016**, *55*, 4361−4366.
(29) Sun, A. C.; Steyer, D. J.; Allen, A. R.; Payne, E. M.; Kennedy, R. T.; Stephenson, C. R. J. A Droplet Microfluidic Platform for High-Throughput Photochemical Reaction Discovery. *Nat. Commun.* **2020**, *11*, No. 6202.
(30) Bitton, A.; Sambrano, J.; Valentino, S.; Houston, J. P. A Review of New High-Throughput Methods Designed for Fluorescence Lifetime Sensing From Cells and Tissues. *Front. Phys.* **2021**, *9*, No. 648553.
(31) Schaaf, T.; Li, A.; Grant, B.; Peterson, K.; Yuen, S.; Bawaskar, P.; Kleinboehl, E.; Li, J.; Thomas, D.; Gillispie, G. Red-Shifted FRET Biosensors for High-Throughput Fluorescence Lifetime Screening. *Biosensors* **2018**, *8*, No. 99.
(32) Chen, Y.-J.; Chen, M.; Hsieh, Y.-C.; Su, Y.-C.; Wang, C.-H.; Cheng, C.-M.; Kao, A.-P.; Wang, K.-H.; Cheng, J.-J.; Chuang, K.-H. Development of a Highly Sensitive Enzyme-Linked Immunosorbent Assay (ELISA) through Use of Poly-Protein G-Expressing Cell-Based Microplates. *Sci. Rep.* **2018**, *8*, No. 17868.
(33) Kandoth, N.; Hernández, J. P.; Palomares, E.; Lloret-Fillol, J. Mechanisms of Photoredox Catalysts: The Role of Optical Spectroscopy. *Sustainable Energy Fuels* **2021**, *5*, 638−665.
(34) Gehlen, M. H. The Centenary of the Stern-Volmer Equation of Fluorescence Quenching: From the Single Line Plot to the SV Quenching Map. *J. Photochem. Photobiol. C: Photochem. Rev.* **2020**, *42*, No. 100338.
(35) O'Brien, C. J.; Droege, D. G.; Jiu, A. Y.; Gandhi, S. S.; Paras, N. A.; Olson, S. H.; Conrad, J. Photoredox Cyanomethylation of Indoles: Catalyst Modification and Mechanism. *J. Org. Chem.* **2018**, *83*, 8926−8935.
(36) Geethanjali, H. S.; Nagaraja, D.; Melavanki, R. M.; Kusanur, R. A. Fluorescence Quenching of Boronic Acid Derivatives by Aniline in Alcohols - A Negative Deviation from Stern-Volmer Equation. *J. Lumin.* **2015**, *167*, 216−221.
(37) Lehrer, S. Solute Perturbation of Protein Fluorescence. Quenching of the Tryptophyl Fluorescence of Model Compounds and of Lysozyme by Iodide Ion. *Biochemistry* **1971**, *10*, 3254−3263.
(38) Azizi, S.; Ulrich, G.; Guglielmino, M.; Le Calvé, S.; Hagon, J. P.; Harriman, A.; Ziessel, R. Photoinduced Proton Transfer Promoted by Peripheral Subunits for Some Hantzsch Esters. *J. Phys. Chem. A* **2015**, *119*, 39−49.
(39) Cukier, R. I.; Nocera, D. G. PROTON-COUPLED ELECTRON TRANSFER. *Annu. Rev. Phys. Chem.* **1998**, *49*, 337−369.
(40) Le, C.; Chen, T. Q.; Liang, T.; Zhang, P.; MacMillan, D. W. C. A Radical Approach to the Copper Oxidative Addition Problem: Trifluoromethylation of Bromoarenes. *Science* **2018**, *360*, 1010−1014.


https://doi.org/10.1021/acsorginorgau.3c00019
*ACS Org. Inorg. Au* 2023, 3, 266−273